Hindawi
Journal of Nanomaterials
Volume 2018, Article ID 8462764, 7 pages
https://doi.org/10.1155/2018/8462764

Research Article

{0 0 1}-Facet-Exposed $Ag_4V_2O_7$ Nanoplates: Additive-Free Hydrothermal Synthesis and Enhanced Photocatalytic Activity

Nguyen Duc Van and Ngo Thi Hong Le

Institute of Materials Science, Vietnam Academy of Science and Technology, 18 Hoang Quoc Viet, Gaugiay, Hanoi 100000, Vietnam

Correspondence should be addressed to Nguyen Duc Van; vannd@ims.vast.ac.vn

Received 10 July 2018; Revised 4 September 2018; Accepted 4 October 2018; Published 31 October 2018

Academic Editor: Nageh K. Allam

The synthesis of silver pyrovanadate, $Ag_4V_2O_7$, nanoplates with exposed {0 0 1}-facets by a facile, additive-free hydrothermal method was described in this paper. The photocatalytic activity of rhodamine B over $Ag_4V_2O_7$ samples under solar light irradiation was also evaluated. By using an equimolar mixture of NH_4VO_3 and $AgNO_3$ with the presence of a suitable amount of ammonia, $Ag_4V_2O_7$ nanoplates were obtained readily and purely at temperatures from 100 to 140°C for 4 h. In particular, the *c*-axis orientation growth of $Ag_4V_2O_7$ nanoplates occurred and increased monotonously with temperatures in the range of over 100 up to 140°C. Further increase in hydrothermal temperature up to 220°C, the $Ag_4V_2O_7$ phase no longer existed and the β-$AgVO_3$ phase was formed instead. The photocatalytic activity of the optimized $Ag_4V_2O_7$ sample comprising {0 0 1}-facet-exposed nanoplates with the highest degree of orientation was significantly higher than that of the random-oriented sample. The effects of using ammonia as a complexing agent on the structure, microstructure, texture, exposed facet, and photocatalytic activity of $Ag_4V_2O_7$ samples were also investigated for the first time.

Dedicated to Assoc. Professor Phan Vinh Phuc on the occasion of his 80th birthday

1. Introduction

Novel ternary oxide-based photocatalysts including silver vanadates as alternatives to traditional TiO_2 have been recently attracted a lot of attention in both basic research and applications [1–4]. For these photocatalytic systems, current research activities focus on enhancing their photocatalytic performances via morphological controlling, crystal facet engineering, and reducing band gap by elemental doping separately or simultaneously [5–9]. The reduction in the average grain size of a photocatalyst from micro- to nanoscale, for instance, was confirmed to enhance the photocatalytic activity due to the increase in its surface area and light absorption [5]. By applying crystal facet engineering, in another approach, the surface energy of textured grains of obtained photocatalytic samples with certain exposed facet is higher than that of random-oriented ones [10–12]. This originated from the fact that the photocatalytic reactivity and efficiency of a photocatalyst are strongly affected by their surface energy and chemisorption properties. Comparing to the case of randomly oriented samples, the photocatalytic process is more accelerated with these textured grains because the adsorption-desorption rates of available species existed on the surface become faster. However, due to their thermodynamic instability with higher surface energy, these highly reactive facets tend to be eliminated during the crystal growth process [13]. To solve this problem, additives were usually employed to tune the growth rates of desired crystal planes [14]. Particularly, for the crystal facet engineering of a powdered photocatalyst prepared by solution chemistry, various chemicals like surfactants [15], ionic liquids [16], or dopants [17] can be used as additives. By using sodium dodecylbenzenesulfonate

(SDBS) and cetyltrimethylammonium bromide (CTAB) as anionic and cationic surfactants, respectively, the ratio of the growth rate along the [1 0 0] direction to that of along [1 1 1] direction of $ZnSnO_3$ can be varied controllably [15]. Recently, ionic liquids were reported to be used as green alternatives to cytotoxic surfactants such as CTAB to control the facet engineering process. By using 1-butyl-3-methylimidazolium tetrafluoroborate ($[Bmim]^+[BF_4]^-$), an ionic liquid, as a morphology-controlling agent, the anatase TiO_2 nanocrystals enclosed by exposed {0 0 1}-facets were obtained via the release of F^- ions from $[BF_4]^-$ anions that stabilized the {0 0 1}-facets, leading to the preferred growth of these facets [16]. In another approach, Yang et al. indicated that the doping of Ta^{5+} ions into rutile TiO_2 crystal lattice enabled tuning of the surface energy of lattice planes and caused induced microstrains that would retard the growth of rutile TiO_2 crystals along the *c*-axis direction. As a result, the Ta^{5+}-doped rutile TiO_2 arrays were grown preferably along [1 1 0] direction, instead of along *c*-axis observed for undoped samples [17]. There are only a limited number of additive-free chemical synthesis procedures of faceted photocatalysts, in which other preparative parameters than additives were exploited for facet engineering so far [18, 19]. Liang et al. synthesized nanoparticle-aggregated cone-like ZnO mesocrystals enclosed by curved $(1\,0\,\bar{1}\,1)$ and flat $(0\,0\,0\,\bar{1})$ surfaces by a water-induced precursor-hydrolysis process in a water/organic solvent system [18]. The results showed that the volume ratio between organic solvent and water played a key role for tailoring the final crystal shape of ZnO with controllable facets. In our recent work, by using freshly produced $Nb_2O_5{\cdot}H_2O$ instead of frequently used, commercialized Nb_2O_5 as a precursor, the *c*-axis-oriented and {0 0 1}-facet-exposed rhombohedral $NaNbO_3$ plate-like microcrystals with enhanced photocatalytic activity were resulted [19]. The formation of the faceted rhombohedral $NaNbO_3$ plate-like microcrystals synthesized by a template-free hydrothermal method was suggested to be attributed to the difference in chemical reactivity between $Nb_2O_5{\cdot}H_2O$ and other polymorphisms of Nb_2O_5. However, the facet engineering research topic has not been yet carried out for silver vanadates in general and silver pyrovanadate, $Ag_4V_2O_7$, in particular [20–23]. In details, most of these works studied the enhancing photocatalytic activities of $Ag_4V_2O_7$-based photocatalysts via controlling their microstructural and morphological properties by a hydrothermal synthesis method. Without using any surfactant, only random-oriented, single crystalline $Ag_4V_2O_7$ microcrystals were obtained [20]. The similar situation was also observed for $Ag_4V_2O_7$-based photocatalytic composites such as $Ag_2O/Ag_3VO_4/Ag_4V_2O_7$ or $Ag_3VO_4/Ag_4V_2O_7$ synthesized by surfactant-free hydrothermal route when only $Ag_4V_2O_7$ powders with microscale sizes were obtained [24, 25]. It is surveyed that there was only one work reported on the sodium dodecyl sulfate-assisted hydrothermal synthesis of the nanosized $Ag_4V_2O_7$ decorated by Ag nanoparticles [26]. To date, to the best of our knowledge, the synthesis and photocatalytic activity of faceted $Ag_4V_2O_7$ in general and {0 0 1}-faceted $Ag_4V_2O_7$ nanosized powders in particular have not yet been reported.

In this work, the additive-free hydrothermal synthesis of $Ag_4V_2O_7$ nanoplates with exposed {0 0 1}-facets from NH_4VO_3, $AgNO_3$, and ammonia was performed for the first time. The photodegradation of rhodamine B (RhB) over these samples under solar light irradiation was also investigated.

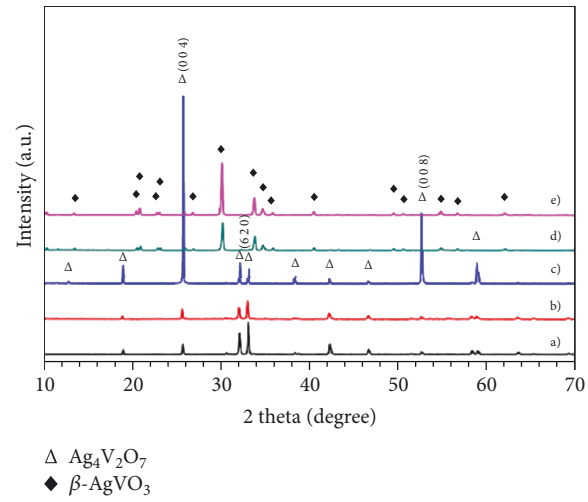

FIGURE 1: XRD diagrams of the samples synthesized at hydrothermal temperature of (a) 100, (b) 120, (c) 140, (d) 160, and (e) 220°C for 4 h.

2. Materials and Methods

2.1. Synthesis of $Ag_4V_2O_7$. For synthesis of $Ag_4V_2O_7$, 0.468 g NH_4VO_3 (Sigma-Aldrich) was firstly dissolved in 50 mL deionized water at 80°C to obtain a yellow solution. This solution was added into a mixture containing 0.68 g $AgNO_3$ (Sigma-Aldrich, 99.5%) and 4 mL of NH_3 (Sigma-Aldrich, p.a.) with different concentrations during stirring. The obtained mixture with the Ag^+/V^{5+} molar ratio of 1 : 1 was transferred into a 125 mL Teflon-lined stainless steel autoclave. The autoclave was filled by deionized water until 80% of its inner volume was occupied, sealed, and heated at a certain temperature for 4 h under autogenous pressure. The samples were filtered, washed several times with deionized water until a neutral pH value was reached, and dried at 50°C for 12 h.

2.2. Characterization Methods. The crystalline structural characterization of the synthesized samples was carried out by X-ray powder diffraction (Bruker D8 Advance diffractometer, CuK_α radiation ($\lambda = 1.5406$ Å)). Their morphological, microstructural, and optical properties were analyzed by using high-resolution transmission electron microscopy (JEOL 2100), field-emission scanning electron microscopy (FE-SEM) (Hitachi S-4800), and UV-Vis diffuse reflectance spectrometry (DR-UV-Vis) (JASCO V670). The photodegradation of rhodamine B over synthesized $Ag_4V_2O_7$ samples was evaluated under solar light irradiation using a solar simulator (Model: 69907, Newport) with the applied light intensity of 100 $mW{\cdot}cm^{-2}$. In details, 0.05 g of the photocatalytic sample was added to 50 mL of the 1.10^{-6} ppm RhB solution. Before being subjected to photocatalytic test, the solution was stirred magnetically for 60 min in the dark to allow the adsorption-desorption

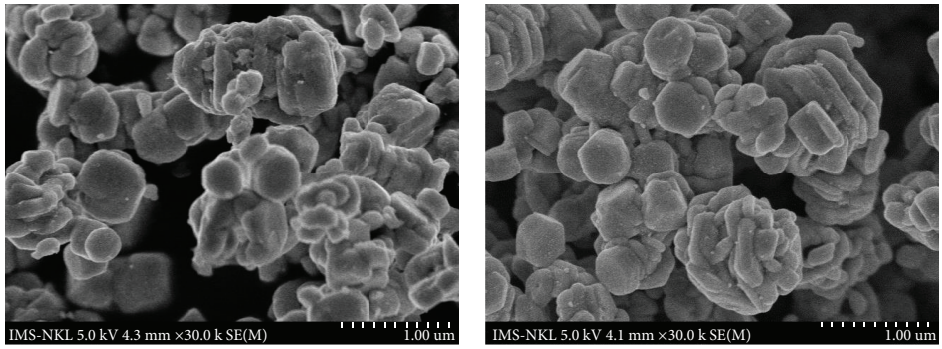

(a) (b)

Figure 2: FE-SEM images of $Ag_4V_2O_7$ samples synthesized at (a) 100 and (b) 140°C for 4 h.

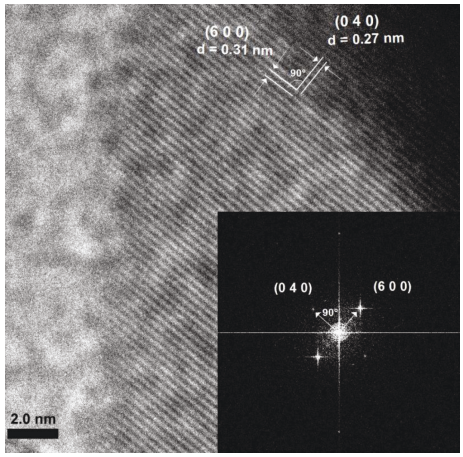

Figure 3: HRTEM image and FFT pattern (inset) of the $Ag_4V_2O_7$ sample synthesized at 140°C for 4 h.

equilibrium to be reached. After every 30 minutes, 3 mL of tested solution was taken and centrifuged to remove the suspended photocatalyst for RhB concentration determination with an aid of a Shimadzu UV-1800 spectrophotometer.

3. Results and Discussion

The crystal phase evolution of samples with different hydrothermal temperatures was performed with results as shown in Figure 1. For samples synthesized at hydrothermal temperatures ranging from 100 to 140°C for 4 h, the pure crystalline orthorhombic phase of $Ag_4V_2O_7$ (ICDD card # 77-0097) was obtained. The most interesting feature is that when temperatures valued at 120 and 140°C, the diffraction intensities of (0 0 4) peak located at 2θ angle of 25.57° became significantly dominated to that of (6 2 0) peak, indicating a *c*-axis crystallographic orientation. The $(I_{(004)}/I_{(620)})$ ratio reached the highest value of 2.5 with the sample synthesized at 140°C in comparison to that of 0.28 documented from the standard pattern of $Ag_4V_2O_7$. However, for the sample autoclaved at 160°C, the $Ag_4V_2O_7$ phase underwent a rapid phase transformation into β-$AgVO_3$ with no trace of $Ag_4V_2O_7$ was detected but the pure β-$AgVO_3$ phase with monoclinic structure (ICDD card # 29-1154) existed instead. This silver metavanadate phase remained uniquely with further increase in reaction temperature up to 220°C.

From SEM images of random- and *c*-axis-oriented $Ag_4V_2O_7$ powders synthesized hydrothermally at 100 and 140°C for 4 h, respectively, the nanoplates were observed in both samples (Figure 2). One can recognized that when the hydrothermal temperature increased from 100 to 140°C, the average diameter and thickness of the plate-like grains increased slightly from 370 to 400 nm and from 54 to 60 nm, respectively. From the HRTEM image and corresponding FFT pattern taken on the surface of $Ag_4V_2O_7$ nanoplates of the sample synthesized hydrothermally at 140°C for 4 h, two orthogonal lattice fringes with the interplanar spacings of 0.31 and 0.27 nm were well indexed to (6 0 0) and (0 4 0) lattice planes of $Ag_4V_2O_7$, respectively (Figure 3). The exposed {0 0 1}-facets of the obtained $Ag_4V_2O_7$ nanoplates were then derived. Thus, in combination with aforementioned XRD results, these observations evidenced that the $Ag_4V_2O_7$ nanoplates favoured to grow along [0 0 1] direction. Based on all above characterization results, it is clear that the single-phase $Ag_4V_2O_7$ nanopowders having relative high homogeneity and well-defined morphology were given at hydrothermal temperatures ranging from 100 to 140°C. This might benefit from using a suitable amount of ammonia and the Ag^+/V^{5+} molar ratio of 1 : 1 with respect to published hydrothermal procedures that always produced $Ag_4V_2O_7$ microcrystals, with or without additives [20, 23]. The autoclaving of an ammonia-free reaction mixture at 140°C for 4 h was also performed with the single-phase powders of β-$AgVO_3$ as as-synthesized product (figure not shown). With the presence of ammonia, in mild basic medium of the hydrothermal mixture, the formation of the desired $Ag_4V_2O_7$ phase can be suggested to differ from that reported in literature and can be described as follows [27, 28]:

$$VO_3^- + OH^- \rightarrow VO_4^{3-} + H^+ \quad (1)$$

$$2VO_4^{3-} + 2H^+ \rightarrow V_2O_7^{4-} + H_2O \quad (2)$$

$$Ag^+ + 2NH_3 \rightarrow \left[Ag(NH_3)_2\right]^+ \quad (3)$$

$$4\left[Ag(NH_3)_2\right]^+ + V_2O_7^{4-} \rightarrow Ag_4V_2O_7 + 8NH_3 \quad (4)$$

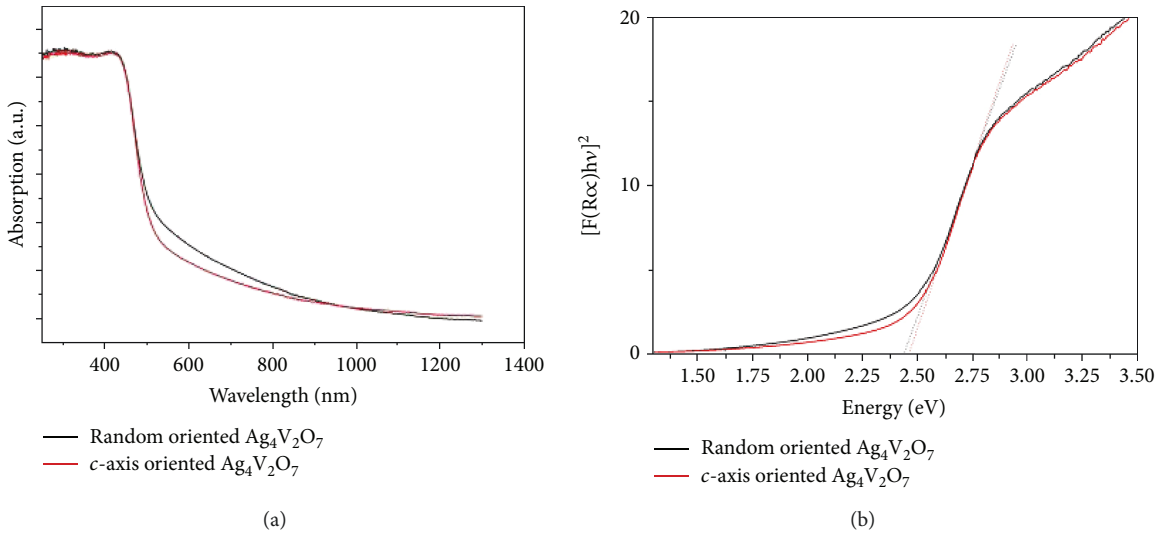

FIGURE 4: (a) DR-UV-Vis spectra and (b) Tauc's plots of the random- and *c*-axis-oriented $Ag_4V_2O_7$ samples.

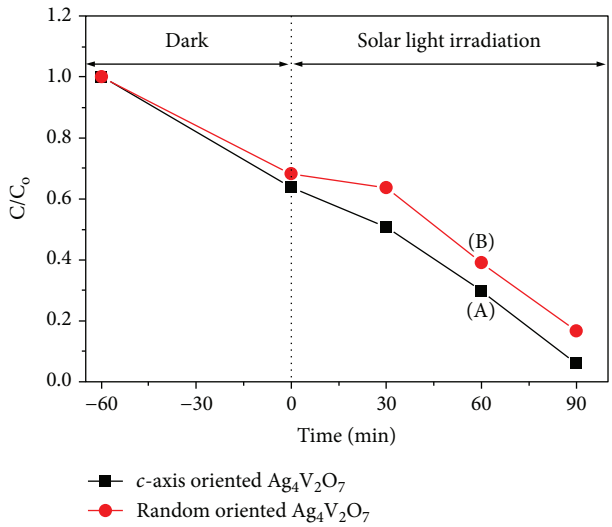

FIGURE 5: Rhodamine B photodegradation efficiency under solar light irradiation over (A) *c*-axis and (B) random-oriented $Ag_4V_2O_7$ samples.

The pH of our reaction mixture was adjusted to over 7 by ammonia solution while this value was remained lower in previous procedures [22, 25]. This enabled a part of ammonia amount to react with Ag^+ ions to form $[Ag(NH_3)_2]^+$ complexes (3). Therefore, the phase formation rate of $Ag_4V_2O_7$ became slower than the case of aqueous Ag^+ ions for the reason that it is necessary for Ag^+ ions to be released from $[Ag(NH_3)_2]^+$ (4), similar to the previous works [29, 30]. This probably facilitates $Ag_4V_2O_7$ crystals of samples synthesized at temperatures ranging from 100 to 140°C to nucleate and grow anisotropically. In addition, the slow release of Ag^+ ions might be also a reason of obtaining the average size of $Ag_4V_2O_7$ plates in nanoscale although no additives were used with respect to the published work [26]. When temperature was increased over 140°C, the β-$AgVO_3$ phase occurred uniquely. It is worthy to note that to obtain the single-phase $Ag_4V_2O_7$ crystals with the highest *c*-axis orientation degree and yield of about 40%, the optimized amount and concentration of ammonia of 4 mL and 2.5 M, respectively, providing the pH of 9.5 for reaction mixture are required strictly. As illustrated in Figure 4, the band gap energy values of the random- and *c*-axis-oriented samples of 2.44 and 2.47 eV, respectively, were almost the same and fell in the range found for $Ag_4V_2O_7$ [19, 20].

The evolution of the RhB photodegradation rate as a function of irradiation time over the random- and *c*-axis-oriented $Ag_4V_2O_7$ samples autoclaved at 100 and 140°C, respectively, was indicated in Figure 5.

After being irradiated for 90 minutes under a solar source, the rhodamine B photodegradation efficiency of 92% was found for the *c*-axis-oriented $Ag_4V_2O_7$ sample while that of the random-oriented sample valued at 71%. From all investigated results, it can be proposed that the grain size and the reactivity of exposed {0 0 1}-facets are two main factors contributing to the enhanced photocatalytic activity of the synthesized samples. However, compared to the case of the random-oriented sample, the higher overall photocatalytic activity that the *c*-axis-oriented $Ag_4V_2O_7$ sample exhibited was probably because their dominated exposed {0 0 1}-facets accelerated the photocatalytic processes on the surface. This can be explained by the fact that although the random-oriented sample possessed a higher size-induced photocatalytic activity than that of the *c*-axis-oriented $Ag_4V_2O_7$ sample comprising larger nanoplates, the facet-induced photocatalytic enhancement dominated over this size-induced one in our study. Thus, for the {0 0 1}-facet-exposed $Ag_4V_2O_7$ sample, both main photocatalytic activity-enhancing solutions for synthesizing nanoscale photocatalysts and crystal facet engineering were combined by simply exploiting the excellent complexing ability of Ag^+ ions with ammonia. For the photodegradation of RhB under visible light irradiation, the photocatalytic efficiency of this faceted $Ag_4V_2O_7$ nanoplates was not only significantly higher than that

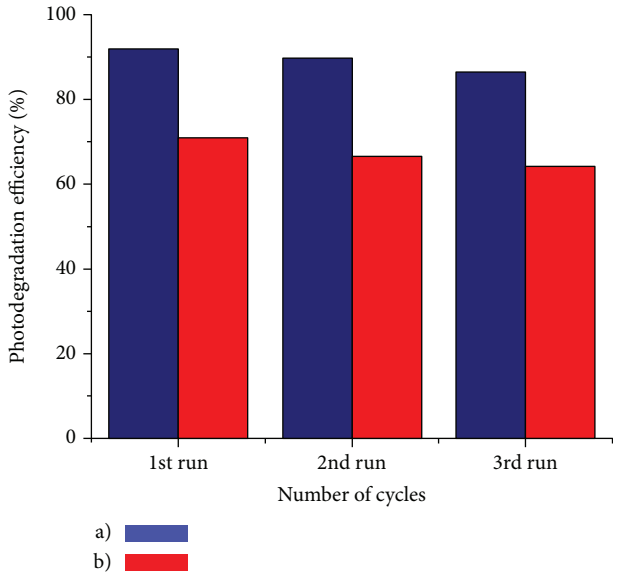

FIGURE 6: Photodegradation recyclability test of rhodamine B over (a) *c*-axis and (b) random-oriented $Ag_4V_2O_7$ samples under solar light irradiation.

reported for silver pyrovanadate [20, 24] but also for other vanadate-based nanophotocatalysts such as Ag_3VO_4, $FeVO_4$, $FeVO_4/V_2O_5$, $BiVO_4$, and $BiVO_4/TiO_2$ [24, 31–33]. Furthermore, in comparison to other novel visible light active ternary oxide-based photocatalysts, it is quite perspective to use our synthesized materials as competitive alternatives to TiO_2 for photodegradation of dyes. This originated from the fact that their photocatalytic activity is distinctive superior to $BiFeO_3$ and $BiFeO_3$-Bi_2WO_6 and comparable to, for example, $Ag_2O/Ag_3VO_4/Ag_4V_2O_7$ and Ag_3PO_4/SBA-15 [24, 34–36]. From these results, it is expected to apply the additive-free facet engineering approach to silver vanadate-based nanophotocatalysts via forming complexes of Ag^+ ions as an intermediate, similar to the case of Ag_3PO_4 [37]. It should be noted that commonly used crystal facet engineering techniques like using template, ionic liquids, or surfactant as structure-directing agents, to a certain extent, are limited for silver-containing photocatalysts due to the ease of reducing and forming undesired insoluble compounds of Ag^+ ions during the synthesis process [9, 38].

Figure 6 demonstrated the recyclability testing results of RhB over the random- and *c*-axis-oriented $Ag_4V_2O_7$ samples for three recycling photocatalytic runs under solar light irradiation. The results revealed that, for *c*-axis-oriented $Ag_4V_2O_7$ sample, the photodegradation efficiency decreased to 89.7% and 86.5% for the second and third cycles, respectively. The similar trend was also observed for the case of the random-oriented sample with photodegradation efficiency of 66.6% and 64.3% for the second and the third cycles, respectively, lower than that of the first cycle (71%). These slight decreases in photodegradation efficiency indicated that both random- and *c*-axis-oriented $Ag_4V_2O_7$ samples are reusable with high stability after three RhB photodegradation cycles.

4. Conclusions

In summary, single-phase silver pyrovanadate, $Ag_4V_2O_7$, nanoplates were synthesized readily by an additive-free hydrothermal method at temperatures from 100 to 140°C by using NH_4VO_3, $AgNO_3$, and ammonia as starting materials. The increase in the hydrothermal temperature facilitates silver pyrovanadate to grow preferably along [0 0 1] crystallographic direction and provided {0 0 1}-facet-exposed nanoplates with the highest *c*-axis orientation degree at 140°C for the first time. The photodegradation efficiency of rhodamine B over random- and *c*-axis-oriented $Ag_4V_2O_7$ samples under solar light irradiation was 71 and 92%, respectively. The enhanced photocatalytic activity of the *c*-axis-oriented $Ag_4V_2O_7$ sample is attributed to their exposed {0 0 1}-facets. This work is expected to provide the possibility to use ammonia as both a pH adjusting agent and a complexing agent to form $[Ag(NH_3)_2]^+$ complexes with Ag^+ ions, allowing photocatalytic crystals to nucleate and grow anisotropically with a slow rate to obtain faceted nanophotocatalysts of silver vanadate and other silver-containing ternary oxides without using any additives.

Data Availability

The datasets used to support the findings of this study are available from the corresponding author upon request.

Conflicts of Interest

The authors declare that there is no conflict of interest regarding the publication of this paper.

Acknowledgments

This research is funded by the Vietnam National Foundation for Science and Technology Development (NAFOSTED) under grant number 104.03-2016.11.

References

[1] M. D. Hernández-Alonso, F. Fresno, S. Suárez, and J. M. Coronado, "Development of alternative photocatalysts to TiO_2: challenges and opportunities," *Energy & Environmental Science*, vol. 2, no. 12, p. 1231, 2009.

[2] R. Konta, H. Kato, H. Kobayashi, and A. Kudo, "Photophysical properties and photocatalytic activities under visible light irradiation of silver vanadates," *Physical Chemistry Chemical Physics*, vol. 5, no. 14, pp. 3061–3065, 2003.

[3] J. M. Song, Y. Z. Lin, H. B. Yao, F. J. Fan, X. G. Li, and S. H. Yu, "Superlong β-$AgVO_3$ nanoribbons: high-yield synthesis by a pyridine-assisted solution approach, their stability, electrical and electrochemical properties," *ACS Nano*, vol. 3, no. 3, pp. 653–660, 2009.

[4] T.-C. Pan, H.-C. Chen, G.-T. Pan, and C. M. Huang, "Photocatalytic oxidation of gaseous isopropanol using visible-light active silver vanadates/SBA-15 composite," *International Journal of Photoenergy*, vol. 2012, Article ID 314361, 8 pages, 2012.

[5] S. Obregón and G. Colón, "On the different photocatalytic performance of $BiVO_4$ catalysts for methylene blue and

rhodamine B degradation," *Journal of Molecular Catalysis A: Chemical*, vol. 376, pp. 40–47, 2013.

[6] G.-T. Pan, M.-H. Lai, R.-C. Juang, T. W. Chung, and T. C. K. Yang, "Preparation of visible-light-driven silver vanadates by a microwave-assisted hydrothermal method for the photodegradation of volatile organic vapors," *Industrial & Engineering Chemistry Research*, vol. 50, no. 5, pp. 2807–2814, 2011.

[7] S. Obregón and G. Colón, "Heterostructured Er^{3+} doped $BiVO_4$ with exceptional photocatalytic performance by cooperative electronic and luminescence sensitization mechanism," *Applied Catalysis B: Environmental*, vol. 158-159, pp. 242–249, 2014.

[8] D. Wang, H. Jiang, X. Zong et al., "Crystal facet dependence of water oxidation on $BiVO_4$ sheets under visible light irradiation," *Chemistry - A European Journal*, vol. 17, no. 4, pp. 1275–1282, 2011.

[9] K. A. Soliman, A. F. Zedan, A. Khalifa et al., "Silver nanoparticles-decorated titanium oxynitride nanotube arrays for enhanced solar fuel generation," *Scientific Reports*, vol. 7, no. 1, p. 1913, 2017.

[10] S. Sun, X. Song, Y. Sun, D. Deng, and Z. Yang, "The crystal-facet-dependent effect of polyhedral Cu_2O microcrystals on photocatalytic activity," *Catalysis Science & Technology*, vol. 2, no. 5, pp. 925–930, 2012.

[11] Y. Ikuma, S. Ogoe, Y. Watanabe, K. Niwa, H. Tajiri, and O. Sakata, "Relationship between the photocatalytic activity and crystallographic orientation of rutile TiO_2 single crystals," *Journal of the Ceramic Society of Japan*, vol. 121, no. 1410, pp. 254–257, 2013.

[12] S. Kumar, R. Parthasarathy, A. P. Singh, B. Wickman, M. Thirumal, and A. K. Ganguli, "Dominant {100} facet selectivity for enhanced photocatalytic activity of $NaNbO_3$in $NaNbO_3$/CdS core/shell heterostructures," *Catalysis Science & Technology*, vol. 7, no. 2, pp. 481–495, 2017.

[13] S. Wang, H. Chen, G. Gao et al., "Synergistic crystal facet engineering and structural control of WO_3 films exhibiting unprecedented photoelectrochemical performance," *Nano Energy*, vol. 24, pp. 94–102, 2016.

[14] G. Liu, J. C. Yu, G. Q. (. M.). Lu, and H.-M. Cheng, "Crystal facet engineering of semiconductor photocatalysts: motivations, advances and unique properties," *Chemical Communications*, vol. 47, no. 24, pp. 6763–6783, 2011.

[15] B. Geng, C. Fang, F. Zhan, and N. Yu, "Synthesis of polyhedral $ZnSnO_3$ microcrystals with controlled exposed facets and their selective gas-sensing properties," *Small*, vol. 4, no. 9, pp. 1337–1343, 2008.

[16] B. Wang, L. Guo, M. He, and T. He, "Green synthesis of TiO_2 nanocrystals with improved photocatalytic activity by ionic-liquid assisted hydrothermal method," *Physical Chemistry Chemical Physics*, vol. 15, no. 24, pp. 9891–9898, 2013.

[17] X. Yang, J. Chen, L. Gong, M. Wu, and J. C. Yu, "Cross-medal arrays of Ta-doped rutile titania," *Journal of the American Chemical Society*, vol. 131, no. 34, pp. 12048-12049, 2009.

[18] S. Liang, X. Gou, J. Cui et al., "Novel cone-like ZnO mesocrystals with co-exposed $(10\bar{1}1)$ and $(000\bar{1})$ facets and enhanced photocatalytic activity," *Inorganic Chemistry Frontiers*, vol. 5, no. 9, pp. 2257–2267, 2018.

[19] N. D. Van, "Template-free synthesis and photocatalytic activity of {0 0 1}-facets exposed rhombohedral $NaNbO_3$ microcrystals," *Ceramics International*, vol. 44, no. 16, pp. 19945–19949, 2018.

[20] J. Wang, X. Yang, J. Chen et al., "Photocatalytic activity of novel $Ag_4V_2O_7$ photocatalyst under visible light irradiation," *Journal of the American Ceramic Society*, vol. 97, no. 1, pp. 267–274, 2014.

[21] C.-M. Huang, G.-T. Pan, Y.-C. M. Li, M. H. Li, and T. C. K. Yang, "Crystalline phases and photocatalytic activities of hydrothermal synthesis Ag_3VO_4 and $Ag_4V_2O_7$ under visible light irradiation," *Applied Catalysis A: General*, vol. 358, no. 2, pp. 164–172, 2009.

[22] R. C. de Oliveira, L. Gracia, M. Assis et al., "Disclosing the electronic structure and optical properties of $Ag_4V_2O_7$ crystals: experimental and theoretical insights," *CrystEngComm*, vol. 18, no. 34, pp. 6483–6491, 2016.

[23] C.-M. Huang, K.-W. Cheng, G.-T. Pan, W.-S. Chang, and T. C.-K. Yang, "CTAB-assisted hydrothermal synthesis of silver vanadates and their photocatalytic characterization," *Chemical Engineering Science*, vol. 65, no. 1, pp. 148–152, 2010.

[24] R. Ran, J. G. McEvoy, and Z. Zhang, "$Ag_2O/Ag_3VO_4/Ag_4V_2O_7$ heterogeneous photocatalyst prepared by a facile hydrothermal synthesis with enhanced photocatalytic performance under visible light irradiation," *Materials Research Bulletin*, vol. 74, pp. 140–150, 2016.

[25] C. Ren, J. Fan, S. Liu et al., "One-step hydrothermal synthesis of novel $Ag_3VO_4/Ag_4V_2O_7$ composites for enhancing visible-light photocatalytic performance," *RSC Advances*, vol. 6, no. 97, pp. 95156–95164, 2016.

[26] J. Wang, J. Chen, Y. Yu et al., "One-step SDS-assisted hydrothermal synthesis and photoelectrochemical study of $Ag_4V_2O_7$ nanorods decorated with Ag nanoparticles," *CrystEngComm*, vol. 17, no. 35, pp. 6661–6668, 2015.

[27] Z. Qu, P. Liu, X. Yang, F. Wang, W. Zhang, and C. Fei, "Microstructure and characteristic of $BiVO_4$ prepared under different pH values: photocatalytic efficiency and antibacterial activity," *Materials*, vol. 9, no. 3, pp. 129–139, 2016.

[28] P. Dong, X. Xi, X. Zhang, G. Hou, and R. Guan, "Template-free synthesis of monoclinic $BiVO_4$ with porous structure and its high photocatalytic activity," *Materials*, vol. 9, no. 8, pp. 685–695, 2016.

[29] R. Dondi, W. Su, G. A. Griffith, G. Clark, and G. A. Burley, "Highly size and shape-controlled synthesis of silver nanoparticles via a templated Tollens reaction," *Small*, vol. 8, no. 5, pp. 770–776, 2012.

[30] D. Li, X. Duan, Q. Qin, H. Fan, and W. Zheng, "Facile synthesis of novel α-Ag_3VO_4 nanostructures with enhanced photocatalytic activity," *CrystEngComm*, vol. 15, no. 44, 2013.

[31] M. Ghiyasiyan-Arani, M. Salavati-Niasari, and S. Naseh, "Enhanced photodegradation of dye in waste water using iron vanadate nanocomposite; ultrasound-assisted preparation and characterization," *Ultrasonics Sonochemistry*, vol. 39, pp. 494–503, 2017.

[32] R. Ran, J. G. McEvoy, and Z. Zhang, "Synthesis and optimization of visible light active $BiVO_4$ photocatalysts for the degradation of RhB," *International Journal of Photoenergy*, vol. 2015, 14 pages, 2015.

[33] Y. Hu, D. Li, H. Wang, G. Zeng, X. Li, and Y. Shao, "Role of active oxygen species in the liquid-phase photocatalytic degradation of RhB using $BiVO_4/TiO_2$ heterostructure under visible light irradiation," *Journal of Molecular Catalysis A: Chemical*, vol. 408, pp. 172–178, 2015.

[34] Z. Chen and W. Jin, "Low-temperature acetone-assisted hydrothermal synthesis and characterization of $BiFeO_3$ powders," *Journal of Materials Science: Materials in Electronics*, vol. 25, no. 9, pp. 4039–4045, 2014.

[35] S. Chaiwichian, K. Wetchakun, W. Kangwansupamonkon, and N. Wetchakun, "Novel visible-light-driven $BiFeO_3$-Bi_2WO_6 nanocomposites toward degradation of dyes," *Journal of Photochemistry and Photobiology A: Chemistry*, vol. 349, pp. 183–192, 2017.

[36] J. Ma, L. Li, J. Zou, Y. Kong, and S. Komarneni, "Highly efficient visible light degradation of rhodamine B by nanophasic Ag_3PO_4 dispersed on SBA-15," *Microporous and Mesoporous Materials*, vol. 193, pp. 154–159, 2014.

[37] H. Wang, L. He, L. Wang et al., "Facile synthesis of Ag_3PO_4 tetrapod microcrystals with an increased percentage of exposed {110} facets and highly efficient photocatalytic properties," *CrystEngComm*, vol. 14, no. 24, pp. 8342–8344, 2012.

[38] G. Xi and J. Ye, "Synthesis of bismuth vanadate nanoplates with exposed {001} facets and enhanced visible-light photocatalytic properties," *Chemical Communications*, vol. 46, no. 11, pp. 1893–1895, 2010.